pTitle: Probing ligand-induced modulation of metallic states in small gold nanoparticles using conduction electron spin resonance

Authors: Anthony Cirri, Alexey Silakov, Lasse Jensen, Benjamin J. Lear*

Affiliations: Department of Chemistry, The Pennsylvania State University, University Park, Pennsylvania, 16802, USA.

*Correspondence to: bul14@psu.edu

Supporting Information

1. Characterization of nanoparticles

The following sections provide the TEM characterization of the hexanethiolate-protected AuNPs, the TEM and UV-Vis characterization of the mixed monolayer protected AuNPs (4-methoxythiophenolate, thiophenolate, 4-bromothiophenolate, or 4-nitrothiophenolate mixed with hexanethiolate), and the NMR quantification of the monolayer composition.

1.i. TEM and UV-visible spectra of the particles.

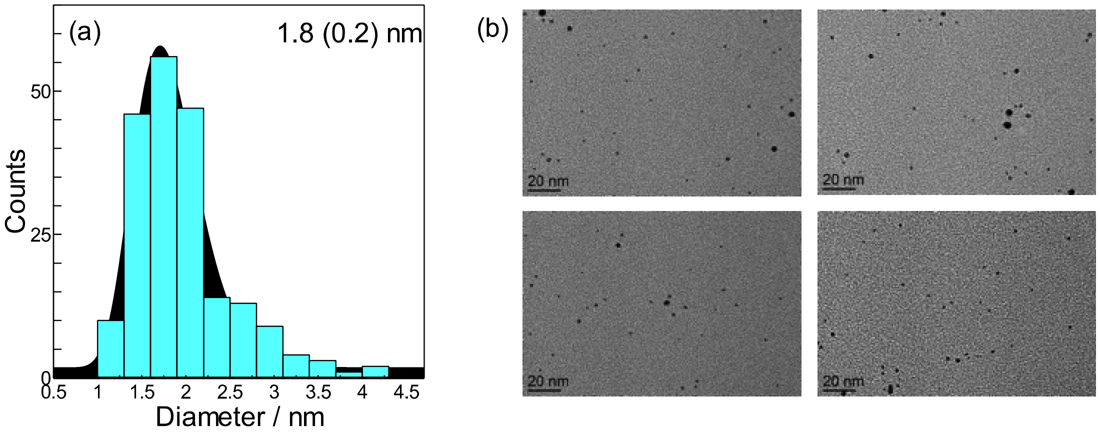

Figure S1. Size distribution (A) and representative TEM micrographs (B) for precursor hexanethiolate-protected AuNPs

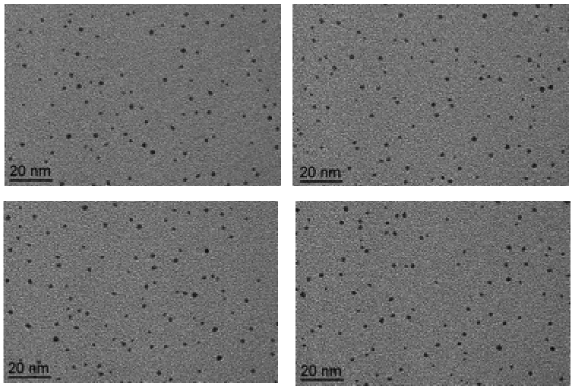

Figure S2. (A) TEM micrographs for 4-methoxythiophenolate-/hexanethiolate-protected AuNPs.

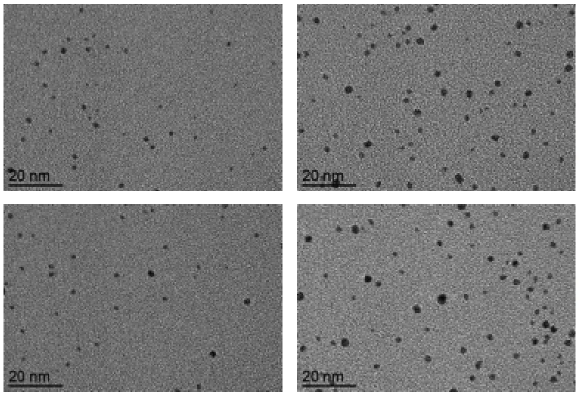

Figure S3. (A) TEM micrographs for thiophenolate-/hexanethiolate-protected AuNPs

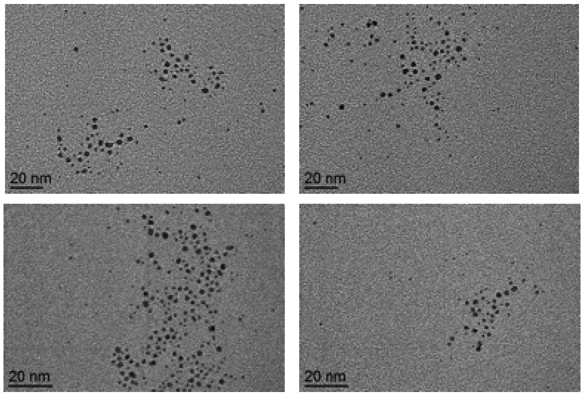

Figure S4. (A) TEM micrographs for 4-bromothiophenolate-/hexanethiolate-protected AuNPs.

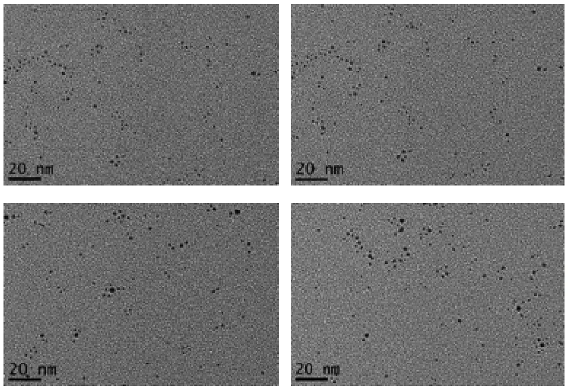

Figure S5. (A) TEM micrographs for 4-nitrothiophenolate-/hexanethiolate-protected AuNPs.

1.ii. Quantifying of percent aromatic ligand coverage on the mixed-monolayer AuNPs

An NMR of the product from the iodine death reaction allowed for quantification of the molar fraction of aromatic thiols, as has been demonstrated by others.(*1*, *2*) Integrated intensities of all hydrogens attached to the aromatic ring and the methyl of hexanethiolate were used to calculate percent compositions. An example for the 4-nitrothiophenolate-containing mixed monolayer AuNPs is given below (Figure S6).

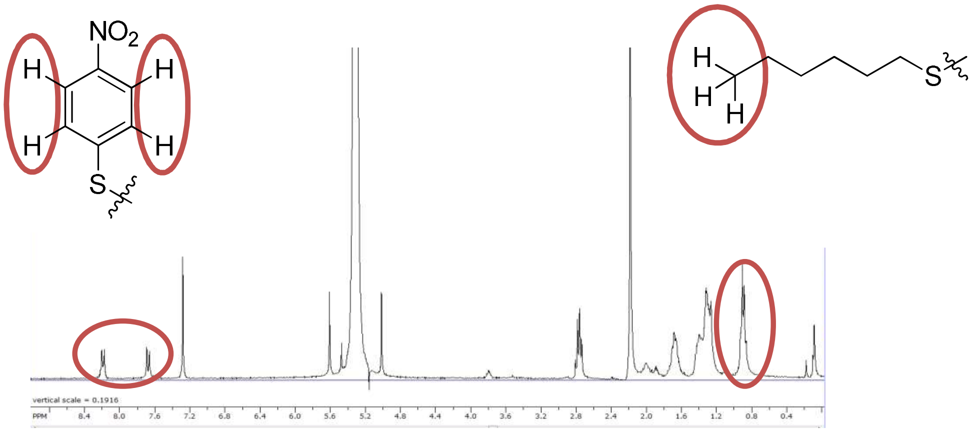

Figure S6. NMR spectrum of ligands cleaved from 4-nitrothiophenolate-/hexanethiolate-AuNPs. The relevant peaks have been circled.

Table S1. Calculation of percent composition for 4-nitrothiophenolate-/hexanethiolate-mixed-monolayer AuNPs

Ligand	Integrated intensity	Relative intensity	Percent composition
4-nitrothiophenolate	4.00	1.00	20.4%
Hexanethiolate	11.7	3.90	79.6%

The relative intensity is calculated by dividing the integrated intensity by the number of hydrogens that the signals correspond to in a single molecule. The percent composition is calculated as the relative intensity divided by the sum of relative intensities, multiplied by 100. The values calculated from Figure S6 are given in Table S1. This same procedure was followed for all nanoparticles.

2. Conduction electron spin resonance (CESR)

2.i. Description

Metals may be viewed as periodic array of cations suspended in a “sea” of delocalized electrons held in electronic bands. Interactions with an applied magnetic field lifts the 0th order degeneracy in the electronic band structure (Zeeman splitting), resulting in an asymmetry inthe number density of electron spins either parallel or anti-parallel to the external magnetic field. Referred to as Pauli paramagnetism, the availability of non-singlet states allows excitation of electronic spins that can be used to produce an ESR signal. The original theory used to describe this behavior was given by Freeman Dyson.(*3*) In his theory, the conductive electrons are approximated as free particles, with individual magnetic moments, capable of diffusing through a solid with Brownian motion. Dyson demonstrated that the ESR signal produced by conducting metal substrates (commonly referred to as the conduction electron spin resonance (CESR) signal) is influenced by the penetration depth of the magnetic excitation field into the metal (skin depth), the electron diffusion time into and out of the skin depth (T_D), the electron-spin relaxation time (T_2), the strength of the external magnetic field (B) and the particle size. In the case of spherical metal nanoparticles where $T_D << T_2$, and the mean free path of the electron is on the order of the skin depth or smaller, the CESR lineshape simplifies to:(*4*)

$$\frac{dP}{dB} = D\,\frac{(1-(\gamma(B-B_o)T_2)^2}{(1+(\gamma(B-B_o)T_2)^2)^2} - A\,\frac{2\gamma(B-B_o)T_2}{(1+(\gamma(B-B_o)T_2)^2)^2} \qquad \text{(S1)}$$

where P is the power absorbed (given as a derivative due to the detection method used in ESR), B_o is the resonance field, γ is the gyromagnetic ratio, and D and A are weighting coefficients for dispersive and absorptive Lorentzian lineshapes, respectively. The dispersive component comes from the fact that the delocalized electrons have a non-zero current density, which produces an effective electric field that the electromagnetic radiation propagates into. The effective electric field of the medium disperses the incoming wave-packet, while the dynamic motion of the electrons leads to damping of the wave. As the ratio of the weighting coefficients, D/A, approaches 0 (A >> D), the lineshape becomes more absorptive, leading to a symmetric Lorentzian first derivative; when D/A > 1, the lineshape becomes more dispersive, leading to a strongly asymmetric lineshape.

2.ii. Fitting procedure

The CESR spectra were fit using the commercially available software, Mathematica 10.0.0, which employed the Levenberg-Marquardt fitting algorithm with default accuracy and precision goals. Due to irregularities in the baseline, a third order polynomial was introduced into Equation S1, giving

$$\frac{dP}{dB} = D\frac{1-(\gamma(B-B_o)T_2)^2}{(1+(\gamma(B-B_o)T_2)^2)^2} - A\frac{2\gamma(B-B_o)T_2}{(1+(\gamma(B-B_o)T_2)^2)^2} - (MB^3 + RB + Z) \qquad \text{(S2)}$$

where M, B, and Z are the adjustable parameters associated with the background correction. This correction gives us the fewest adjustable parameters, while providing us with a simulation that gives consistent results regardless of the range of magnetic fields included in the fitting window. In all cases, the spectra were background subtracted (using a spectrum of THF without AuNPs measured under the same conditions) and normalized. An initial guess of 0.33 T and 1 x 10^{-10} s for B_o and T_2, respectively, and 1 for all other adjustable parameters (D, A, M, R, Z) was submitted as the initial guess. A sample spectrum fitted to Equation S2 (prior to subtraction of the background) is given in Figure S7 for **2’** (see manuscript for sample details), and a summary of the extracted parameters are given in Table S2. For clarity, the CESR signal, the cubic background, and the sum of the two are superimposed on Figure S7.

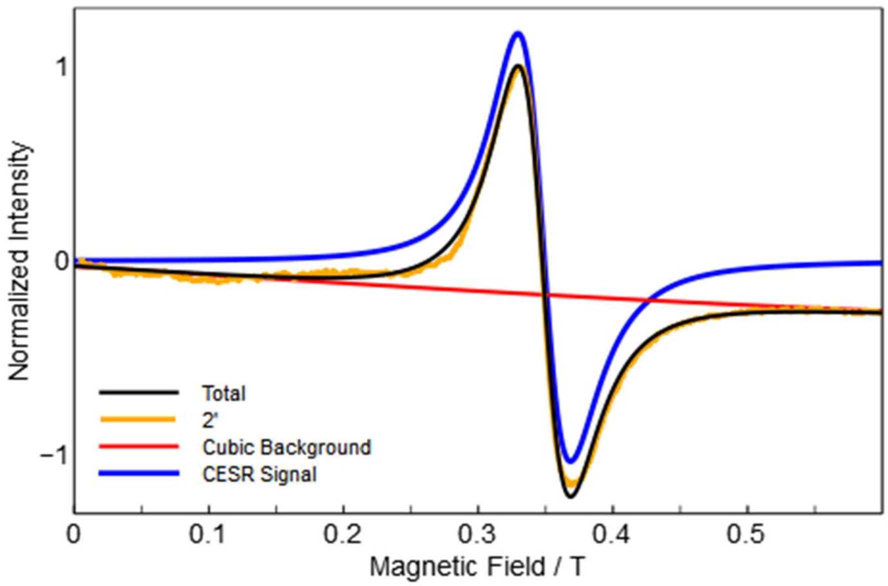

Figure S7. Normalized CESR spectrum of sample **2’** as recorded by our instrument (orange line) with the fitted CESR signal (blue line), cubic background (red line), and the sum of the two (black line) superimposed.

Table S2. Parameters extracted from the fits of CESR spectra for the AuNPs protected by the ligands listed below.

	B_o / T	**T_2 / (10^{-10} s)**	**D**	**A**	**M**	**R**	**Z**
4-methoxythiophenol	0.34813	10.3029	0.326388	1.92955	0.552768	0.959352	0.46
Thiophenol	0.34653	10.5100	0.264162	1.68645	0.025634	0.076206	0.12
4-bromothiophenol	0.34302	10.2090	0.79222	2.30152	0	0	0
4-nitrothiophenol	0.33282	9.90702	0.685991	3.03062	0.325000	0.218754	0.06
4-methoxythiophenol[a]	0.34842	9.80566	0.246095	1.53089	-0.589234	0.683039	-0.1392
4-methoxythiophenol[b]	0.34857	9.89491	0.214068	1.53915	-1.0333	1.18938	-0.33
Thiophenol[c]	0.346206	9.02368	0.468017	1.23794	-0.41935	0.549021	-0.1245
4-bromothiophenol[d]	0.334126	8.04867	0.515056	1.34314	-0.009529	-0.077039	0.11127

a. Spectrum in Figure S8a; b. Figure S8b; c. Figure S8c; d. Figure S8d

2.iii. Additional CESR spectra and origin of error

In order to assess the reproducibility of the ligand control over the CESR spectrum, a second set of particles protected with 4-methoxythiophenol, thiophenol, and 4-bromothiophenol were prepared and analyzed. Additionally, a second sample of the 4-methoxythiophenol-containing AuNPs was prepared in order to approximate the overall experimental error associated with each measurement. The spectra are given in Figure S8.

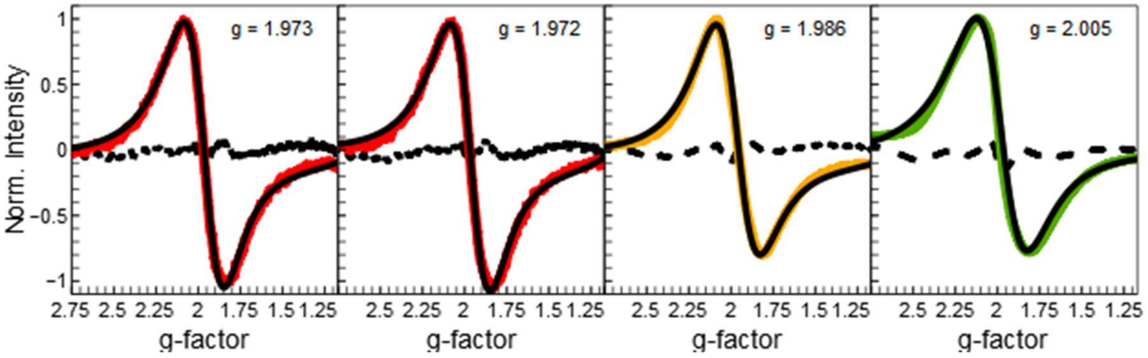

Figure S8. CESR spectra of mixed monolayer AuNPs protected with (a, b) 4-methoxythiophenol, (c) thiophenol, and (d) 4-bromothiophenol.

From the data obtained for the 4-methoxythiophenol AuNPs, we find that the overall experimental error in the g-factor is on the order of 0.001; this error is assumed for all measurements. The error was estimated from repetition of measurements on a single sample. Following the same analysis provided in the manuscript, we can calculate $\Delta g_{surface}$ (Table S3), and we find that we reproduce our previous results very well, on a sample-by-sample basis.

Table S3. Size, % aromatic ligand coverage, and CESR for additional AuNPs in reproducibility study

	Size / nm	**% aromatic ligand coverage**	**g-factor**	**$\Delta g_{surface}$**
OMe	1.8 (0.1)	46%	1.973 / 1.972	-0.088 / -0.089
H	1.9 (0.3)	50%	1.986	-0.076
Br	1.8 (0.2)	27%	2.005	-0.056

2.iv. Discussion of T_2

At the low temperatures we have employed for this study, the dominant mechanism for inducing spin relaxation is collision with lattice defects (including the surface of the metal).(*5*) For each collision, there is a probability of transition of the excited electron from the α to the β spin manifold. For small particles, there are two competing effects of size upon the spin lifetime.(*3*) As the size of a metallic particle decreases from the bulk, the electrons will encounter the surface of the particle with ever-increasing frequency – and this will lead to faster electron spin relaxation. Thus, one initially expects to observe decreasing T_2 with decreasing size. However, at a certain size (dependent upon the metal) the T_2 will begin to *increase* with decreasing size.(*3*) The reason for this is that, for small enough nanoparticles, the electronic bands cease to be continuous, and energy gaps appear between k-vectors. Once the gap between electronic levels becomes comparable to the Zeeman splitting, there is no longer a guarantee of a k-vector in the β manifold that is of appropriate energy to accommodate the energy given off by the return of an electron from the α manifold. That is, due to the emergence of discrete electronic energy levels within small particles the energy conservation requirement is no longer automatically met. This reduces the probability of a spin flip with each collision, and increases the observed T_2. The T_2 will continue to increase as the particle dimensions decrease (and the energy spacing between k-vectors increases) until the system arrives at the value of T_2 for an isolated metal atom.

Because of these effects, we expect that there will be a strong dependence of T_2 upon the size of the nanoparticles (controlling discrete nature of states) and their ligand set (controlling the energy spacing and alignment of the states); further work on a larger number of size-varying systems will be needed to fully deconvolute the impact of the size and ligand set on T_2. For now, we simply note that the values we measure are not unexpected, and are similar for other (alkali) metal systems.(*3*) For those metal systems, the smallest value of T_2 was found for particles *much* larger than those that we investigate(*3*) – however, we also note that the strong spin-orbit coupling of the gold system will delay the onset of the discrete energy states until particle sizes that are *much* smaller than for the light alkali metals.

2.v. g-shift (Δg)

The measured g-value of the nanoparticles was extracted from the resonance field position of the measured ESR spectra, using the following equation

$$\Delta E = h\nu = g\beta B_o \tag{S3}$$

where h is Planck's constant, ν is the frequency of the microwave excitation field, g is the g-factor, β is the Bohr magneton, and B_o is the observed resonance field extracted from the fit.

The main discussion of the results focuses on the g-factor, in terms of the g-shift from the free electron value of approximately 2.0023. The reason is that the observed g-factor provides a sensitive probe of the environment explored by the metallic electrons *(6)*. Changes to the nature of the electronic states via modification of the band structure, surface potential, work function, or surface structure will result in changes to the observed g-factor. This is the reason for focusing on the g-factor (or g-shift).

2.v.a. Size and ligand dependence of the g-shift

The g-shift (additive deviation from the free electron g-factor, ~2.0023) for conduction electrons in metal nanoparticles is also dependent on size. This is due to the fact that the g-factor for pure gold must vary between that for bulk gold and for an isolated atom of gold, as the particle size varies from bulk to single atom. Therefore, in order to compare the measured g-shift for the four AuNPs, we will assume that the bulk of the signal comes from the mean-sized particles and correct for size using Equation S4.

$$\Delta g_{size} = f_{surface}\Delta g_{atom} + (1 - f_{surfa}\quad)\Delta g_{bulk} \tag{S4}$$

Here, Δg_{size} is the expected g-shift due to size, $f_{surface}$ is the fraction of metal atoms at the surface, Δg_{bulk} is the measured g-shift of the bulk metal (0.10 ± 0.01), and Δg_{atomic} is the g-shift of the isolated metal atom (1.8×10^{-3}).(*3*) This expression has been shown to be valid for other metal particulate systems *(7)*. Using data compiled by Murray and co-workers, we calculated the number of gold atoms for our AuNPs.(*8*) Figure S9 shows the calibration curve that we generated form Murray's data,(*8*) and which we used for this calculation.

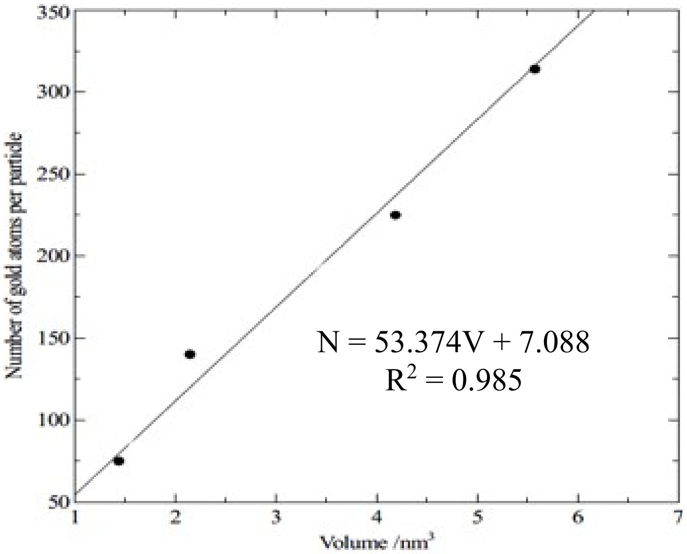

Figure S9. Gold atoms per particle as a function of spherical particle volume. Data was obtained from the work of Murray and co-workers.(*8*)

Upon estimating the number of gold atoms present in each particle, we then calculated the number of surface atoms present, using the equation for an icosahedron:

$$f_{surface} = \frac{N_S}{N_T} = \frac{4{N_T}^{2/3}}{(1+4/{N_T}^{1/3})}\left(\frac{1}{N_T}\right) \tag{S5}$$

where N_S and N_T are the number of surface atoms and the total atoms, respectively. Equation S5 was then used to derive the size- dependence in the g-shift. The data obtained from the calibration curve, Equation S4, and Equation S5 is summarized in Table S4. Data experimentally measured by Murray and co-workers for the core number is retained in the table and highlighted in grey.

Table S4. AuNP size, total atom count, surface atom count, and g-shift due to size for a bare gold particle

Diameter / nm	$\mathbf{N_T}$	$\mathbf{N_S}$	$\mathbf{\Delta g_{size}}$
2.2	314	116	0.064
2.1	271	104	0.062
2.0	225	89	0.061
1.9	202	82	0.060
1.8	173	72	0.059
1.7	147	63	0.058
1.6	140	61	0.057
1.5	103	47	0.055
1.4	75	37	0.052

Lastly, it is assumed that the observed g-shift, $\Delta g_{\text{observed}}$, is a linear combination of the g-shift due to size, Δg_{size}, and the g-shift due to the action of the ligand, Δg_{ligand} (Equation S6).

$$\Delta g_{observed} = \Delta g_{size} + \Delta g_{ligand} \tag{S6}$$

We use Equation S6 to isolate the effect of the ligand on the g-shift of the particle. The rational for this approach lies in the perturbative treatment of effect of spin-orbit coupling over the g-factor, where it can be shown that the observed g-shift is composed of a linear combination orbital angular momenta mixing of the ground state wave-function and nearby orbitals, or k-states in the case of solid-state materials *(6)*. In this context, Equation S6 is the grouping of the contributions (from the linear combination to the g-shift) that arise from (*i*) the orbitals associated with the metallic gold core (Δg_{size}) and (*ii*) the new states that come from the surface chemistry (Δg_{ligand}).

3. UV-Vis Spectra

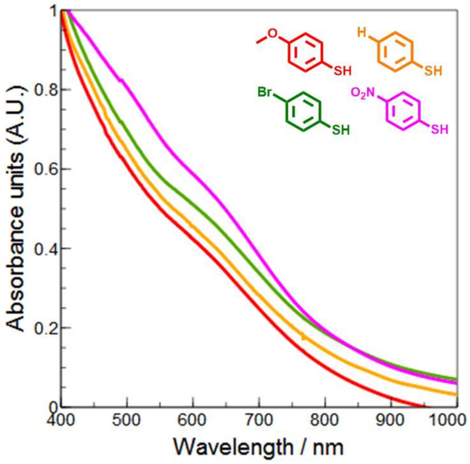

Figure S10. UV-Vis spectra for **1'** (red), **2'** (orange), **3'** (green), and **4'** (magenta). See the main text for sample designations.

4. Experimental Methods

4.i . Materials

Chloroauric acid trihydrate ($HAuCl_4 \cdot 3H_2O$; 99.999% purity) and 4-bromothiophenol were purchased from Acros Organics. 4-nitrothiophenol was purchased from Oakwood Chemicals. Tetraoctylammonium bromide (TOAB) was purchased from Merck. Hexanethiol (95%), thiophenol, and 4-methoxythiophenol were purchased from Sigma Aldrich. All solvents were purchased from VWR International. All chemicals were used as purchased without further purification.

4.ii. Synthesis of hexanethiolate-protected AuNPs

The synthesis of hexanethiolate-protected AuNPs followed a modified two-phase Brust approach.[9] Initially, TOAB (2.19 g, 4.00 mmol) was suspended in 60 mL of toluene, and the solution was stirred vigorously until the phase transfer agent was completely dissolved. $HAuCl_4 \cdot 3H_2O$ (345 mg, 0.900 mmol) was dissolved in 25 mL of deionized water and added to the organic solution, where the two-phase solution was stirred until complete transfer of the gold precursor occurred (10 minutes). Once complete, the aqueous phase was discarded, and hexanethiol (0.4 mL, 2.81 mmol) was added, where a color change from red-orange to white was observed. Once the color change was complete, 25 mL of a freshly prepared 0.1 M aqueous sodium borohydride (384 mg, 10.1 mmol) was added drop-wise to a vigorously stirring solution of the gold-hexanethiol mix. A color change from white to near-black was observed immediately, and the solution was left to stir for three hours.

To purify the particles, the aqueous phase of the two-phase reaction was discarded and 400 mL of methanol was added to the toluene solution. The resulting suspension was placed in the freezer for two hours, and the solid collected. The solid was washed with methanol (5 mL x 3), and the filtrate discarded. The dried AuNPs were collected (brown solid, typical yield: 200 mg).

4.iii. Ligand exchange

All surface-modification syntheses followed the same synthetic scheme and only a general procedure will be described here.[1,2] Hexanethiolate-protected AuNPs (100 mg) were dissolved in THF (50 mL). The para-substituted aromatic thiol (0.347 mmol) was then added to the solution, and the mixture was stirred for 4 hours. At the conclusion of the reaction, the solvent was removed via rotary-evaporation, and the particles were re-suspended in a minimal amount of THF. Sufficient methanol (200 mL) was then added to crash out the AuNPs. In the case of ligand exchange with bromothiophenol, acetone (200 mL) is used instead of methanol. The suspension was placed into the freezer overnight, and the resulting solid was collected. The solid was washed with methanol (5 mL x 8), dried, and collected (brown solid, typical yield: 90 mg).

4.iv. Iodine death reaction

To quantify the relative concentration of ligands on the mixed-monolayer surface, the alkyl and aromatic ligands were cleaved from the surface using iodine.[10] Briefly, the surface-modified AuNPs were suspended in dichloromethane (50 mL), and an excess of iodine was added (0.100 g). The solution immediately turned violet, and was stirred for 30 minutes. After, the solution was filtered through a fine-fritted filter and rotary-evaporated to dryness. No further purification was performed.

4.v. Characterization of AuNPs

TEM

Nanoparticles were sized using JEOL2010 TEM with a LaB6 emission source and an accelerating voltage of 200 kV. The samples were prepared by drop-casting dilute solutions of the AuNPs in dichloromethane onto carbon-coated copper mesh grids, purchased from Electron Microscopy Sciences.

Raman Spectroscopy

Raman spectra were acquired using a Renishaw inVia Raman Microscope. The surface-modified AuNPs were analyzed with a 647 nm CrystaLaser CL-2000 diode pumped laser (70 mW at 10% power, model DL647-070) and a 1200 l/mm grating was used to resolve the spectra (1.9 cm^{-1} resolution). The samples were prepared by drop-casting the AuNPs onto a glass substrate from a concentrated THF solution and dried using a stream of nitrogen.

UV-Vis Spectroscopy

UV-Vis spectra were acquired on an Agilent 8453 UV-Vis spectrometer. A quartz cuvette with a 1 cm path length was used for all measurements. All spectra were recorded in THF and diluted such that the maximum absorption was below 1 absorption unit.

CW-CESR Spectrsocopy

CW-CESR measurements were performed using a Bruker ESP 300 X-band spectrometer with an ER 041MR microwave bridge. A dual-mode ER 4116DM cavity operated in the perpendicular TE102 microwave mode (ν_{MW} = 9.623 GHz) was used to collect all spectra. Temperatures 25 K and below were achieved using an ER 4112-HV Oxford Instruments variable temperature helium flow cryostat. All measurements were performed using the following parameters: microwave power, 200 mW; modulation amplitude, 2 G; time constant, 40.96 ms; conversion time, 81.92 ms; number of points, 4096. Saturated solutions of AuNP samples were prepared with THF, degassed by sparging with argon, and sealed with paraffin wax tape in clear fused quartz tubes with 4mm O.D./3mm I.D.

^{1}H NMR Spectroscopy

^1H NMR spectra were acquired on a Bruker DPX 300 MHz spectrometer. The samples were prepared by dissolving the residue from the iodine death reaction in $CDCl_3$. No purification was performed on the residue.

4.vi. Computational Details

All calculations presented in this work were performed using a local version of the Amsterdam Density Functional (ADF) program package.[11,12] The geometries were optimized using a TZP basis set and the BP86 functional. Solvent effects were accounted for using COSMO![13] and scalar relativistic effects were included using the zeroth-order regular approximation (ZORA).[14,15] The ionization potential (IP) was calculated as the energy difference between the $Au_{25}(SR)_{18}^-$ and $Au_{25}(SR)_{18}$ for the clusters. For the ligands, the IP was calculated as the energy difference between H-SR and H-SR$^+$.

5. References

1. Song, Y., Murray, R.W. Dynamics and extent of ligand exchange depend on electronic charge of metal nanoparticles. *J. Am. Chem. Soc.* **124**, 7096 – 7102 (2002).

2. Tang, Z. *et al.* Mixed dithiolate durene-DT and monothiolate phenylethanethiolate protected Au_{130} nanoparticles with discrete core and core-ligand energy states. *J. Am. Chem. Soc.* **133**, 16037 – 16044 (2011).

3. Halperin, W.P. Quantum size effects in metal particles. *Rev. Mod. Phys.* **58**, 533 – 606 (1986).

4. Edmonds, R.N., Edwards, P.P., Guy, S.C., Johnson, D.C., Electron-spin resonance in small particles of sodium, potassium, and rubidium metals. *J. Phys. Chem. B* **88**, 3764 – 3771 (1984).

5. Edmonds, R.N., Harrison, M.R., Edwards, P.P. Chapter 9. Conduction electron spin resonance in metallic systems. *Annu. Rep. Prog. Chem., Sect. C* **82**, 265 – 308 (1985).

6. Weil, J.A. & Bolton, J.R. *Electron Paramagnetic Resonance: Elementary Theory and Practical Applications, 2nd Edition* (Wiley-Interscience, New York, 2007).

7. Buttet, J., Car, R., Myles, C.W. Size dependence of the conduction-electron-spin-resonance g shift in a small sodium particle: orthogonalized standing-wave calculation. *Phys. Rev. B*

26, 2414 – 2431 (1982).

8. Wolfe, R.L., Balasubramanian, R., Tracy, J.B., Murray, R.W. Fully ferrocenated hexanethiolate monolayer-protected gold clusters. *Langmuir* **23**, 2247 – 2254 (2007).

9. Brust, M., Walker, M., Bethell, D., Schiffrin, D.J., Whyman, R. Synthesis of thiol-derivatised gold nanoparticles in a two-phase Liquid–Liquid system, *J. Chem. Soc., Chem. Comm.*, 801 – 802 (1994)

10. Templeton, A.C., Hostetler, M.J., Kraft, C.T., Murray, R.W. Reactivity of monolayer-protected gold cluster molecules: Steric effects, *J. Am. Chem. Soc.*, **120**, 1906—1911 (1998)

11. te Velde, G., Bickelhaupt, F.M., Baerends, E.J., Guerra, C.F., van Gisbergern, S.J.A., Snijders, J.G., Ziegler, T. Chemistry with ADF, *J. Comput. Chem.*, **22**, 931—967, (2001)

12. Guerra, C.F., Snijders, J.G., te Velde, G. , Baerends, E.J. Towards an order-N DFT method, *Theor. Chem. Acc.*, **99**, 391—403 (1998)

13. Klamt, A., Schüürmann, G., COSMO: a new approach to dielectric screening in solvents with explicit expressions for the screening energy and its gradient, *J. Chem. Soc., Perkin Trans. 2*, 799—805 (1993)

14. van Lenthe, E., Baerends, E.J., Snijders, J.G., Relativistic regular two-component Hamiltonians, *J. Chem. Phys.*, **99**, 4597—4610 (1993)

15. . van Lenthe, E., Baerends, E.J., Snijders, J.G., Relativistic total energy using regular approximations, *J. Chem. Phys.*, **101**, 9783—9792 (1994)

Supplementary Material:

Figures S1-S10

Tables S1-S4

References (*1-15*)